VERTICAL BRIDGMAN CONFIGURATION HEATED FROM BELOW:
3D BIFURCATION AND STABILITY ANALYSIS

R. BENNACER[1], M. Ei GANAOUI[2], E. LEONARDI[3]

[1] LEEVAM, Univ. Cergy-Pontoise, 5 mail Gay Lussac, Neuville sur Oise 95031, France

[2] SPCTS, Fac. Sciences et Techniques, Univ. Limoges, 123 Albert Thomas, 87060 Limoges, France

[3] The University of New South Wales, Sydney, Australia 2052

ABSTRACT

Phase change is of great importance in the materials and crystal growth processes. The control of this phenomena permits growth of high quality pure crystals. Most papers on Bridgman crystal growth configurations present two-dimensional (2D) or axisymmetric calculations. Recently three-dimensional (3D) computations have been limited to high Prandtl number. This study focuses on the three-dimensional character of low Prandtl number flows and on symmetry breaking phenomena which can produce some unsteadiness in the flow and consequently perturb the solid/liquid interface shape and dopant distribution. Only the hydrodynamics in the melt is analyzed in this paper. In past papers the critical stability limit for the onset of the natural convection in two-dimensional flows was undertaken and the threshold value for breaking symmetry and unsteadiness were identified. In the present work, this problem is studied using three-dimensional simulations thus overcoming the limitation of the 2D assumption. It has been found that the initially steady symmetric flow in the 3D case becomes asymmetric for lower Ra number than for the 2D case. The breaking in symmetry occurs firstly in the transverse plane. For the relatively low Ra number we still have no intensification in the global heat transfer but it appears that the heat transfer increases locally on the bottom and decreases on the vertical active walls. The classical spiral flows typical for the 3D effect (in the third direction) is also identified.

NOMENCLATURE

A_x x aspect ratio, L_x/L_z
A_y y aspect ratio, L_y/L_z
g gravitational acceleration [m s^{-2}]
h dimensionless heating height, scaled using L_z
L_x dimension of cavity in x direction [m]
L_y dimension of cavity in y direction [m]
L_z dimension of cavity in z direction [m]

Nu_{down} Nu on bottom wall $= \int_{y=0}^{1} \int_{z=0}^{1} \frac{\partial \theta}{\partial x}\Big|_{x=0} dy\,dz$

Nu_{up} Nu on top wall $= \int_{y=0}^{1} \int_{z=0}^{1} \frac{\partial \theta}{\partial x}\Big|_{x=1} dy\,dz$

Nu_{Lat} Nu on lateral walls $= \int_{y=0}^{1} \int_{x=0}^{1} \frac{\partial \theta}{\partial x}\Big|_{z=0,1} dy\,dx$

Pr Prandtl number, $= \nu/\alpha$
Ra Rayleigh number, $= g\ \beta_T\ \Delta T\ L_z^3\ /(\nu\alpha)$
T dimensional temperature [K]
u, v, w x, y, z components of dimensionless velocity
x, y, z dimensionless Cartesian coordinates of system

Greek symbols

α thermal diffusivity [m^2 s^{-1}]
β_T coefficient of volumetric expansion [K^{-1}]
θ dimensionless temperature, $=(T-T_C)/(T_H-T_C)$
μ dynamic viscosity [kg m^{-1} s^{-1}]
ν kinematic viscosity [m^2 s^{-1}]
ρ density [kg m^{-3}]

INTRODUCTION

Investigation of stability for melt flows under crystal growth conditions permits one to qualify the critical operating parameters of crystal growth. Hence there has been increased interest in the flows of liquids metals in cavities subjected to external temperature gradients.

Stable dynamic solutions are important for practical applications because of their impact on the constitutional control (dopant distribution). During solidification of binary alloys the thermal and concentration buoyancy forces either aid (or oppose) each other, depending on the type of alloy and process of the heating (and cooling).

Fluids heated from below exhibit very strong non-linear behaviour which is of the interest in many scientific fields. The classic Rayleigh-Bénard problem offers a first approach to studying the complexity of the flow, which evolves from a conductive solution to a convective one and it can be considered as the first predictive method of coupling with the solid/liquid transition. For example, in the electronic industry, interface shape is strongly affected by convection (Brice 1976).

2D models are commonly used for predictive numerical investigation of directional solidification configurations based on solutal control (Mc Fadden and Coriell 1987, Impey and Riley 1991), under low gravity conditions (Alexander *et al.* 1991) or on the thermal control (Larroudé *et al.* 1994).

In these cited works a 2D model was utilized for both the restricted fluid phase and full solidification model. Computational results presented in these papers were used to analyze a dynamic regime interacting with the

solid/liquid transition. Recent extensions to 3D calculations (Lan and Wang 2001) are limited to high Prandtl number and do not cover the extensive situations encountered in real crystal growth.

In this study we focus on thermal natural convection which induces symmetry breaking for low Prandtl number material. The configuration considered by the authors in a previous works (El Ganaoui 1998, Kaenton *et al* 2003) is extended here to the 3D case.

MODEL AND NUMERICAL METHOD

The problem under consideration is sketched in Figure 1. It consists of a Cartesian domain filled with a low Prandtl number liquid metal (*Pr =0.01*), heated from below and cooled from the top. The left and right walls are heated up to the level of the height *h (=H/Lz)* and are adiabatic in the remaining part (*1-h*). The front and the rear walls are set to be adiabatic.

Governing equations

The thermo physical properties of the fluid are treated as constants. Newtonian and laminar flow is assumed and the Boussinesq approximation has been used, in which the liquid density is assumed to be constant except in the buoyancy term of the momentum equation.

We introduce the following non-dimensionalisation,

$$x = x'/L_z, \quad y = y'/L_z, \quad z = z'/L_z, \quad \tau = t'L_z^2/\nu$$
$$u = u'L_z/\nu, \quad v = v'L_z/\nu, \quad w = w'L_z/\nu, \quad P = P'L_z^2/\rho\nu^2$$
$$\theta = (T - T_C)/(T_H - T_C)$$

in which L_z is the length of the cavity in the z direction, ν is the kinematic viscosity, ρ is the fluid density and T_H and T_C are the hot and cold wall temperatures respectively.

With the above assumptions and dimensionless variables, the governing equations to be solved can be written as,

Continuity

$$\frac{\partial u}{\partial x} + \frac{\partial v}{\partial y} + \frac{\partial w}{\partial z} = 0 \qquad (1)$$

X-Momentum

$$\frac{\partial u}{\partial \tau} + u\frac{\partial u}{\partial x} + v\frac{\partial u}{\partial y} + w\frac{\partial u}{\partial z} = -\frac{\partial P}{\partial x} + \frac{Ra\theta}{Pr} + \nabla^2 u \qquad (2)$$

Y-Momentum

$$\frac{\partial v}{\partial \tau} + u\frac{\partial v}{\partial x} + v\frac{\partial v}{\partial y} + w\frac{\partial v}{\partial z} = -\frac{\partial P}{\partial y} + \nabla^2 v \qquad (3)$$

Z-Momentum

$$\frac{\partial w}{\partial \tau} + u\frac{\partial w}{\partial x} + v\frac{\partial w}{\partial y} + w\frac{\partial w}{\partial z} = -\frac{\partial P}{\partial z} + \nabla^2 w \qquad (4)$$

Energy

$$\frac{\partial \theta}{\partial \tau} + u\frac{\partial \theta}{\partial x} + v\frac{\partial \theta}{\partial y} + w\frac{\partial \theta}{\partial z} = \frac{1}{Pr}\nabla^2\theta \qquad (5)$$

The non-dimensional parameters are the Prandtl number $Pr = \nu/\alpha$ and Rayleigh number, $Ra = g\,\beta_T\,\Delta T\,L_z^3/(\nu\alpha)$.

Velocity is assumed to be no slip on the entire boundary of the domain and the temperature boundary conditions are:

$$\theta(0,y,z) = 1$$
$$\theta(x,y,0) = \theta(x,y,1) = 1 \quad for \quad 0 < x < h$$
$$\left.\frac{\partial\theta}{\partial x}\right|_{(x,y,0)} = \left.\frac{\partial\theta}{\partial x}\right|_{(x,y,1)} = 0 \quad for \quad h < x < 1$$
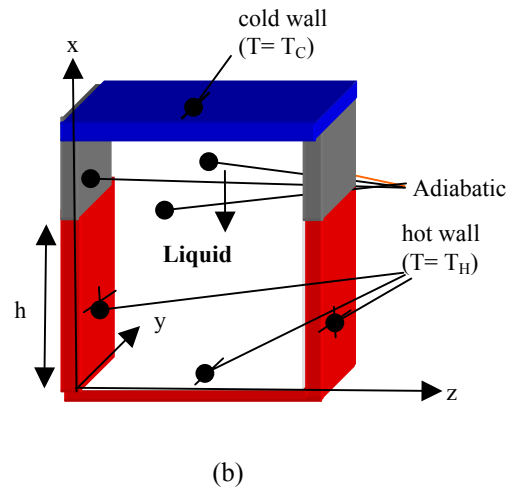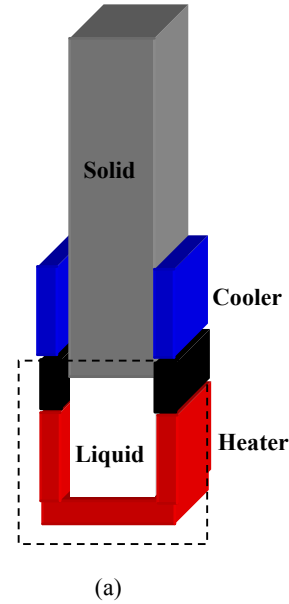$$\theta(1,y,z) = 0$$

(a)

(b)

Figure 1: Schematic diagram of (a) the physical domain and (b) the simplified configuration studied.

Method of solution

Equations (l-5) are approximated by using a staggered, non-uniform control volumes grid, and a third order accurate QUICK scheme (Leonard 1979) for the advection terms. ULTRA-SHARP (Leonard and Mokhtari 1990, Leonard and Drummond 1995) flux limiter is used to remedy any non-physical oscillations. The SIMPLE algorithm is used to couple momentum and continuity

equations. The momentum equations are solved by the implicit procedure (SIP), which is extended here to handle 3D problems. The discretization of the pressure correction equation results on a symmetric coefficient matrix that is solved using the conjugate gradient (CG) method. The coefficient matrix resulting from the discretization of the energy equation is non-symmetric and is solved iteratively by the BI-CGSTAB method. SSOR preconditioning is used for accelerating the convergence rates of both the CG and the BI-CGSTAB methods. To reduce the high computer times inherent in the solution of 3D natural convection problems, a full approximation storage (FAS) full multigrid (FMG) method (Sezai and Mohamad 2000) is applied to the problem.

The equations are solved by a four level fixed V-cycle procedure starting at the coarsest grid level and progressing to the finer grid level. A tri-linear interpolation is used for all variables, an area weighted average procedure is used for all quantities defined on the control-volume surface (such as velocities) and a volume weighted average procedure is adopted for all quantities defined at the control-volume centre such as pressure and temperature. For time dependant problems, a second order accurate Euler scheme is used.

In this work 82x82x82 (and 102x102x102) irregular grids are used on the finest level. The non-uniform grids have denser clustering near the surface boundaries. The computational code was validated by comparison with the numerical results of Mukutmoni and Yang (1993) and the 3D test case presented in (Bennacer *et al.* 2001).

RESULTS AND DISCUSSION

The effect of the heating size parameter on the resulting heat transfer on the bottom and top of the cavity are presented in the figure 2. Transfers rates are not equal, except for $h = 0$ case, because of the additional heating on the two lateral walls ($z = 0$ and $z = 1$). The upper heat transfer balances the contribution of the lower and two lateral surfaces.

For $Ra = 3x10^3$, the transfer is mainly diffusive with weak flow and it is totally conductive for the $h=0$ case.

The difference between the average heat transfer on the lower and the upper surface increases with h because of the increasing contribution of the two lateral surfaces. For considerable heating sizes (h) the main transfer is from the side to upper part with a very small contribution from the bottom surface. This conclusion is valid during the mainly conductive regime.

The effect of Rayleigh number on the heat transfer at the top of the cavity is presented in Figure 3 for different h values. For lower Ra the resulting Mussel number Nu is constant and corresponds to the previously discussed diffusive heat transfer.

For a given Ra number the increasing in h induces higher transfer which is not equal to 1, except for $h=0$, since we used a one dimensional diffusive heat transfer given by $q_{ref} = \lambda (T_H - T_C)/L_X$ as the reference heat flux. Above certain Ra numbers (corresponding to the appearance of the convective solutions) an increase in the heat transfer is observed. The transitional Ra value depends on h.

It should be noticed that the case $h=0$ corresponds to the standard Rayleigh-Bénard bifurcation problem. In this case one main cell, due to the heating at the bottom wall, is obtained. This cell can rotate either clockwise or counter-clockwise and also in the diagonal plane depending on the governing parameters. Figure 4 shows the local heat transfer coefficients (Nu number) on the hot bottom surface for different Ra in the transitional range. The local heat transfer distribution can be used to illustrate the flow pattern where the higher Nu values correspond to the location of the impacting jet on the surface and the lower Nu values to the location of the rising flow. The isocontours of the local heat transfer on the bottom ($x=0$) correspond to one rotating main cells inside the cavity under three situations: a diagonal one in the z-x and y-x planes.

The wavelength and the pattern of the obtained flow depend on several parameters: this is beyond the scope of the present study.

The global transition from diffusive to convective solution (Fig. 3) seems to be similar for the different cases.
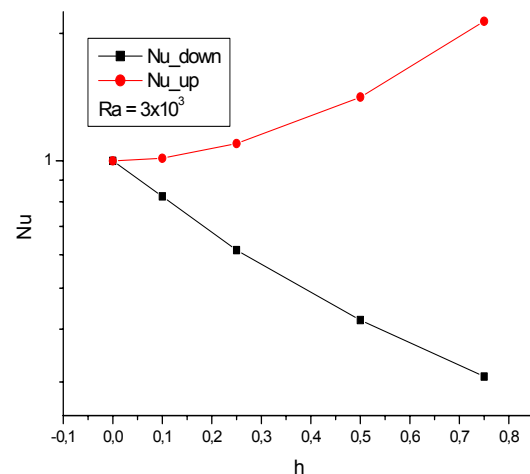

Figure 2: Heat transfer on upper and lower surfaces for different heating sizes h ($Ra=10^3$, $A_x=A_y=1$).
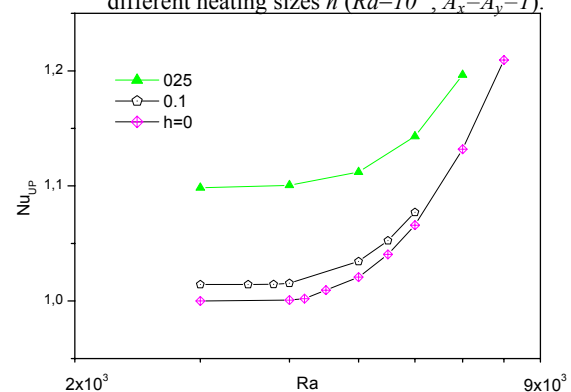

Figure 3: Heat transfer as a function of Ra on the upper surface for different heating sizes h ($A_x=A_y=1$)

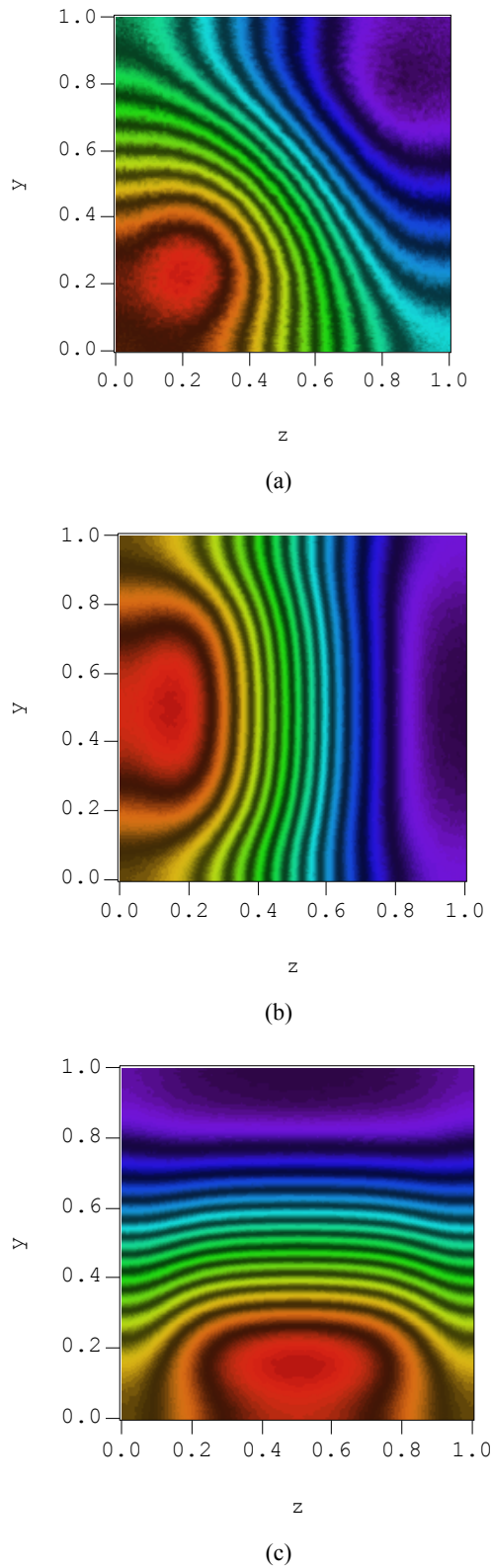Nevertheless it is clear that lateral heating modifies the flow structure.

(a)

(b)

(c)

Figure 4: The local Nusselt number on the hot-lower surface, for $h=0$, at different Ra, (a) 4×10^3, (b) 4.5×10^3 and (c) 5×10^3.

The temperature field is presented in figure 5(a), showing cooling on the upper surface, heating on the bottom surface and the two vertical surfaces, and the adiabatic areas.

The hot fluid goes up along the heating vertical plate and moves down in the vertical x-y mid-plan. The flow consists of two counter-rotating main cells inside the cavity, as shown in figure 5(b) by the stream-trace in the vertical x-z mid-plane. This motion brings cold fluid from the top to the bottom wall through the core of the cavity (see figure 5(b)). The resulting flow for this Ra exhibits a weak spiral flow, which is similar to a 2D flow structure in a very deep cavity.

Increasing the Ra number (in the lower Ra range) modifies the flow intensity without significantly affecting the overall heat transfer (Fig. 3) but it does modify the ratio between lateral and lower surface contributions (Table 1).

				Nu			
Ra	10^0	10^1	10^2	10^3	2×10^3	3×10^3	4×10^3
Down	0.258	0.258	0.260	0.279	0.304	0.310	0.337
Lat.	0.69	0.69	0.69	0.69	0.686	0.684	0.68
Top	-2.10	-2.10	-2.10	-2.12	-2.13	-2.14	-2.15

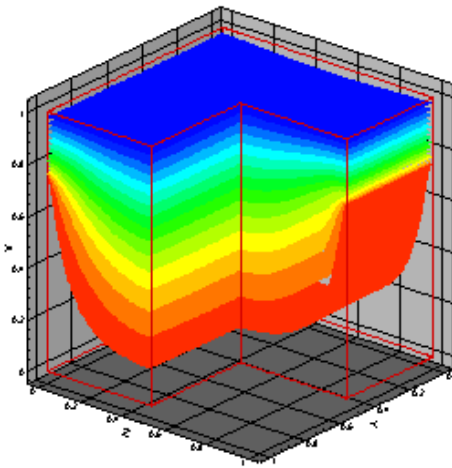**Table 1**: Nu for different Ra ($A_x=A_y=1$); $h = 0.75$

The resulting symmetric regimes (previously discussed) exhibit increases in the flow intensity with Ra and h. The flow looses this symmetry for $Ra = 4\times10^3$. This feature is seen in the figure 6. This figure shows isocontours of local heat transfer on the bottom horizontal surface ($x=0$) for different Ra and represents four different situations:

For low Ra ($\leq 10^1$), solutions exhibit a diffusive temperature field (Fig. 6(a)). The maximum gradient is in the middle due to the imposed thermal boundary conditions.
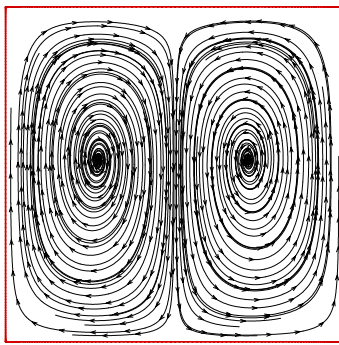
For intermediate Ra, the increase in the flow induces higher local Nu in the centreline due to arriving of the cold fluid. The effect of the third direction is obvious as the friction, close to the $y=0$ and 1 walls, damps the flow, so that the local transfer is lower. See figure 6(b). The maximum heat transfer is in the centre of the surface.

For $Ra = 3\times10^3$ we have a break in the symmetry in the transversal direction (figure 6(c)) which appears earlier than in the 2D case and is in the plane perpendicular to the one obtained in the 2D case. The vertical y-x mid-plane symmetry vanishes and a full 3D solution is obtained. For this situation we still have a particular symmetrical field in the x-z mid-plane and the vertical line ($y=z=0.5$) corresponds to a symmetrical line. For higher Ra (4×10^3) we have a global non-symmetrical flow with the main flow moves either to front plan ($y=0$) or rear plane ($y=1$).

The third case with symmetrical line consists of two counter-rotating rolls in the y direction. The rolls are of equal sizes in the middle vertical plane x-z and a non-equal size behind and in front to the plane. An example of
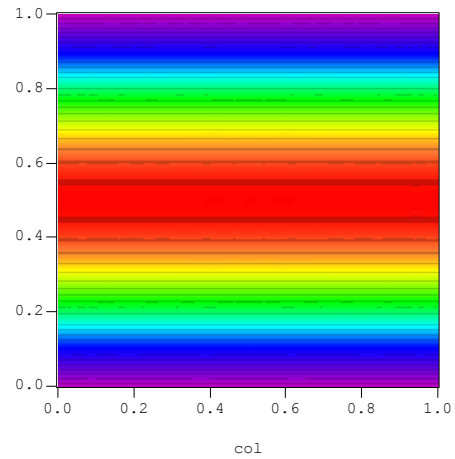
y

(a)

(b)

Figure 5: (a) The 3D temperature field and (b) Stream traces at the (*y=0.5*) lateral plane *x-z*, for *Ra = 1x10³*.
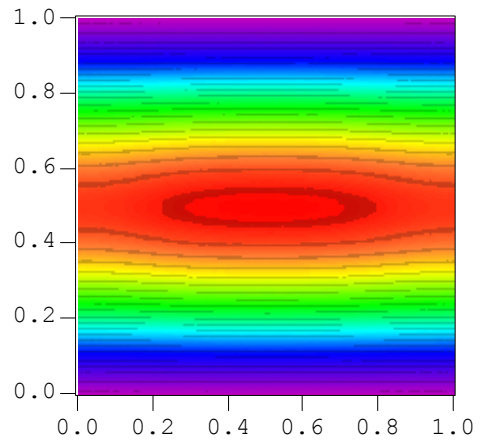
such a situation is illustrated on figure 7 where stream traces are represented on three different planes (*y= 0.15, 0.5* and *0.85*). The flow shape versus the depth is obvious and this explains the local heat transfer distribution illustrated before in figure 6.

For the 2D case we have a symmetrical solution until *Ra* = 5000 and an asymmetric one for *Ra* ≥ 7000. It became unsteady for *Ra* > 30000 and periodic for *Ra* > 40000 (El Ganaoui *et al.* 1998). In the 3D case the asymmetric and unsteady case appear for lower *Ra* in comparison to the 2D approach.
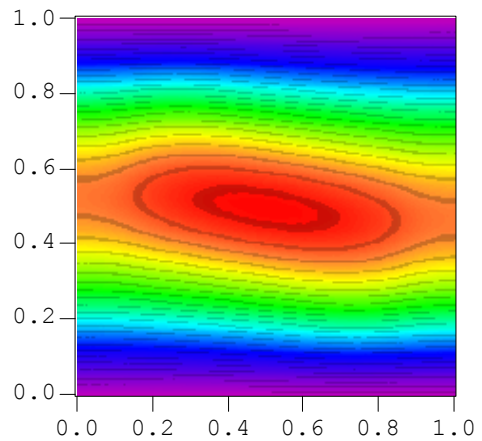
The asymmetric solution could be due to the chosen aspect ratio. Analysing the effect of the depth of the cavity, a 2D asymmetrical flow is obtained for low A_y and fully 3D for high A_y. The depth dependency illustrates clearly the existence of wave-length effects in the *y* direction. The flow is similar to the one shown in figure 7 for L_Y =1 (cubical case), however it is more asymmetric. These result give a clear explanation of the asymmetric steady state solution obtained using the 2D assumption. This solution is the one obtained in front and behind the central symmetric plane.

col

(a)

(b)

(c)

Figure 6: Local Nusselt number on the hot-lower surface (*y-z* plane) for different *Ra*, (a) *1x10¹*,(b) *2x10³* and (c) *3x10³*.
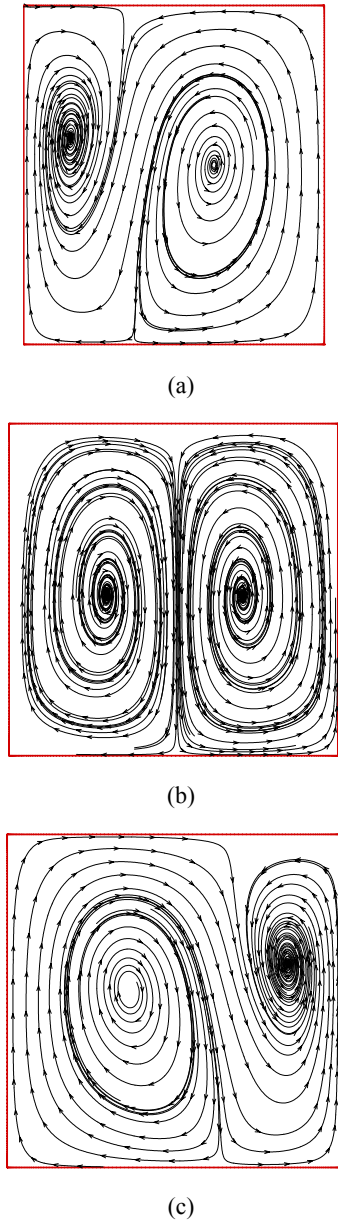
(a)

(b)

(c)

Figure 7: Stream traces at different lateral planes
(a) *y=0.15*, (b) *y=0.5* and (c) *y=0.85*, for
$Ra = 3 \times 10^3$, $Pr = 0.01$ and cubical cavity.

CONCLUSION

In this work three dimensional computations of a simplified phase change problem in a vertical Bridgman configuration heated from below are presented. The effect of the *Ra* number, the heating size *h* (furnace size) and the aspect ratio L_Y on the flow structure and heat transfer distribution is analyzed. A comparison of the 3D results with a previous 2D approach has been discussed and the resulting differences in the appearance of breaking in symmetry for lower *Ra* (and in the transversal plane) is presented. This analysis also illustrates the limitation of the 2D assumption in identifying such transitions. The flow becomes 3D for relative low *Ra* and the preliminary results illustrate the effect of the depth of the cavity on the mean flow and the existence of a wavelength in the third direction.

REFERENCES

ALEXANDER, J., AMIROUDINE, S., OUAZZANI, J. and ROZENBERGER, F., (1991), "Analysis of the low gravity tolerance of Bridgman-Stockbarger crystal growth II. Transient and periodic accelerations", *J. Crystal Growth,* **113**, 21-38.

BENNACER, R., MOHAMAD, A.A. and SEZAI, I., (2001), "Transient natural convection in air-filled cubical cavity: Validation Exercise", *CHT'01 Advances in Computational Heat Transfer II*, G. de Vahl Davis and E. Leonardi (eds), Begell House Inc., New York, 1385-1390.

BRICE, J.C., (1976), *The growth of crystals from liquids*. North-Hollands, New York,.

EL GANAOUI, M. and BONTOUX, P., (1998), "An Homogenisation Method for Solid-Liquid Phase Change During Directional Solidification", R.A. Nelson, T. Chopin, and S.T. Thynell (eds.), *Numerical and Experimental Methods in Heat Transfer, ASME H.T.D.*, **361,** (5), 453-469.

IMPEY, M.D., RILEY, D.S., WHEELER, A.A. and WINTERS, K.H., (1991), "Bifurcation analysis of solutal convection during directional solidification", *Phys. Fluids A*, **3**, 535.

KAENTON, J., SEMMA, E., TIMCHENKO, V., EL GANAOUI, M., LEONARDI, E., and DE VAHL DAVIS, G., (2003), "Effects of anisotropy and solid/liquid thermal conductivity ratio on flow instabilities during inverted Bridgman growth". Submitted to *Numerical Heat Transfer*.

LAN C.W. and WANG C.H., (2001), "Three-dimensional bifurcations of a two phases Rayleigh-Benard problem in a cylinder". *Int. J. Heat and Mass Transfer*, **44**, 1823-1836.

MCFADDEN, B. and CORIELL, S.R., (1987), "Thermosolutal convection during directional solidification. II. Flow transitions", *Phys. Fluids*, **30**, 659-671.

LARROUDÉ, PH., OUAZZANI, J., ALEXANDER, J.I.D. and BONTOUX, P., (1994). "Symmetry breaking flow and oscillatory flows in a 2D directional solidification model." *European Journal of Mechanics - B/Fluids*, **13**, (3), 353-381.

LEONARD, B.P., (1979), "A stable and accurate convective modeling procedure based on quadratic upstream interpolation", *Comput. Methods Appl. Mech. Eng*, **19**, 59-98.

LEONARD, B.P. and MOKHTARI, S., (1990), "Beyond first order upwinding: the ULTRA-SHARP alternative for non-oscillatory steady-state simulation of convection", *Int. J. Numerical Methods Eng*, **30**, 729-766.

LEONARD B.P. and DRUMMOND J.E., (1995), "Why you should not use 'Hybrid', 'Power-Law' or related exponential schemes for convective modelling: there are much better alternatives", *Int. J. Num. Method. Fluids*, **20**, 421-442.

MUKUTMONI, D. and YANG, K.T., (1993), "Rayleigh-Bénard convection in a small aspect ration enclosure. Part I: Bifurcation to oscillatory convection", *J. Heat Transfer*, **115**, 360-366.

SEZAI, I. and MOHAMAD, A.A., (2000), "Natural convection from a discrete heat source on the bottom of a horizontal enclosure", *Int. J. Heat Mass Transfer*, **43**, 2257-2266.